Journal of Materials Chemistry C

ROYAL SOCIETY OF CHEMISTRY

PAPER

View Article Online
View Journal | View Issue

Cite this: J. Mater. Chem. C, 2023, 11, 7299

Circularly polarized luminescence in the one-dimensional assembly of binaphtyl-based Yb(III) single-molecule magnets†

Carlo Andrea Mattei, [a] Vincent Montigaud,[a] Bertrand Lefeuvre,[a] Vincent Dorcet,[a] Gilles Argouarch, [a] Olivier Cador, [a] Boris Le Guennic, [a] Olivier Maury, [b] Claudia Lalli, [a] Yannick Guyot,[c] Stéphan Guy,[c] Cyprien Gindre,[c] Amina Bensalah-Ledoux,[c] François Riobé,*[bd] Bruno Baguenard*[c] and Fabrice Pointillart *[a]

Received 9th March 2023,
Accepted 2nd May 2023

DOI: 10.1039/d3tc00858d

rsc.li/materials-c

Lanthanide ions have attracted great interest owing to their optical and magnetic properties. Single-molecule magnet (SMM) behavior has been a fascinating science for thirty years. Moreover, chiral lanthanide complexes allow the observation of remarkable circularly polarized luminescence (CPL). However, the combination of both SMM and CPL behaviors in a single molecular system is very rare and deserves attention in the design of multifunctional materials. Four chiral one-dimensional coordination compounds involving 1,1′-Bi-2-naphtol (BINOL)-derived bisphosphate ligands and the Yb(III) centre were synthesized and characterized by powder and single-crystal X-ray diffraction. All the Yb(III)-based polymers displayed field-induced SMM behavior with magnetic relaxation occurring by applying Raman processes and near infrared CPL in the solid state.

Introduction

Potential applications in high-density data storage,[1] quantum computing[2] and spintronics[3] are making single-molecule magnets (SMMs) very appealing owing to their slow magnetic relaxation and magnetic bistability. Since the discovery of such a magnetic phenomenon for a terbium mononuclear complex, lanthanides have been holding a central place in the design of SMMs. Such an important role was recently reinforced by the observation of blocking temperature near the liquid nitrogen boiling temperature for a series of lanthanide organometallic complexes.[4–7] Moreover, lanthanide ions are well-known for their specific optical properties with emission line-like spectra and long emission lifetimes ranging from microseconds to milliseconds.[7–10] Such characteristics open the routes to applications in bioimaging,[11–13] optical telecommunication devices[14–18] or material science, for instance, OLED.[19,20] In the context of molecular magnetism, the lanthanide luminescence could be helpful because it can be observed as a photograph of the energy diagram of the ground-state multiplet under crystal field interaction, and thus it can be correlated to the magnetic properties,[21–23] especially in the case of luminescent SMMs.[24–29] The association of two or more physical properties could lead to the appearance of a new phenomenon. One of the most known associations concerns chirality and magnetism leading to the observation of magneto-chiral dichroism (MChD).[30] When the system displays slow magnetic relaxation, chiral SMMs,[31] ferroelectric SMMs,[32] chiral luminescent SMMs[33–37] and magneto-chiral SMMs[38,39] can be obtained. In the specific case of chirality-luminescence association, circularly polarized luminescence (CPL) can be detected and defined as the difference in intensity between the emissions of left- and right-circularly polarized light.[40,41] CPL active materials have interest for potential applications in 3D-displays,[42] data storage[43] and biomolecular processes.[44,45] The CPL activity is commonly expressed by the dissymmetry factor g_{lum} defined as $g_{lum} = 2(I_L - I_R)/(I_L + I_R)$, where I_L and I_R represent the intensity of the left- and right-circularly polarized emissions, respectively. Thus, the g_{lum} factor ranges from −2 to +2 limits. However, g_{lum} commonly ranges from 10^{-4} to 10^{-2} for chiral organic molecules.[46–48] Further, lanthanide ions are ideal candidates for

[a] Univ Rennes, CNRS, ISCR (Institut des Sciences Chimiques de Rennes) – UMR 6226, 35000 Rennes, France. E-mail: fabrice.pointillart@univ-rennes1.fr
[b] Univ Lyon, ENS de Lyon, CNRS UMR 5182, Laboratoire de Chimie, 69342, Lyon, France
[c] Univ Lyon, Université Claude Bernard Lyon 1, CNRS, UMR 5306, Institut Lumière Matière, 69622 Lyon, France. E-mail: bruno.baguenard@univ-lyon1.fr
[d] Univ. Bordeaux, CNRS, Bordeaux INP, ICMCB, UMR 5026, F-33600 Pessac, France. E-mail: francois.riobe@icmcb.cnrs.fr

† Electronic supplementary information (ESI) available: SCXRD and PXRD data, computational details, ac magnetic data, absorption and CD data. CCDC 2238387–2238389. For ESI and crystallographic data in CIF or other electronic format see DOI: https://doi.org/10.1039/d3tc00858d

CPL observation owing to their allowed magnetic dipole transitions (provided that $\Delta J = 0, \pm 1$), leading to large rotatory strengths compared with the electric dipole ones. Therefore, a remarkable g_{lum} factor[49] could be measured for Cs[Ln((+)-hfbc)$_4$] complex (where hfbc = 3-heptafluorobutylryl-(+)-camphorato) (Ln = Eu(III), g_{lum} = 1.38;[50] Ln = Yb(III), g_{lum} = 0.38[51]), [(Binol)$_3$ErNa$_3$] (where Binol = 1,1′-Bi-2-naphtol) (g_{lum} = 0.47)[52] and [(*R*-Spinol)$_3$LnNa$_3$(thf)$_6$] (where Spinol = 1,1′-spirobiindane-7,7′-diol) (Ln = Sm(III), g_{lum} = 0.50; Tb(III), g_{lum} = 0.53 and Dy(III), g_{lum} = 0.53).[53]

To combine the SMM and CPL properties, we investigated different couples of rare earth ions and chiral ligands. We recently published a series of Dy(III) and Eu(III) polymeric structures involving BINOL-derived bisphosphate ligands with axial chirality.[54–56]

The Dy(III) derivatives displayed slow magnetic relaxation, while the Eu(III) displayed CPL properties in both the solution and solid states. To screen different sources of chirality, we also studied chiral dipicolinamide (metal-centred chirality),[57] β-diketonate (point chirality)[58] and helicenic (helical chirality)[59] ligands associated with the Yb(III) ion. In fact, the Yb(III) ion seems to be an ideal candidate because it has a significant magnetic anisotropy and a unique $^2F_{5/2} \rightarrow {}^2F_{7/2}$ magnetic dipole transition. Therefore, in our quest for the best materials combining CPL and SMM, we investigate a new Yb(III) series involving four binaphtyl-based ligands (Scheme 1). In this study, we present the X-ray structures, chiroptical and magnetic properties of {[Yb(hfac)$_3$((*S*)/(*R*)-L^1)]$_3$}$_n$ (**[(*S*)/(*R*)-1]$_n$**), {[Yb(hfac)$_3$((*S,S,S*)/(*R,R,R*)-L^2)]$_3$}$_n$ (**[(*S,S,S*)/(*R,R,R*)-2]$_n$**), {[Yb(hfac)$_3$((*S*)/(*R*)-L^3)]$_3$}$_n$ (**[(*S*)/(*R*)-3]$_n$**) and {[Yb(hfac)$_3$((*S,S,S*)/(*R,R,R*)-L^4)]$_3$}$_n$ (**[(*S,S,S*)/(*R,R,R*)-4]$_n$**).

Results and discussion

Structural analysis

Recently, we reported the X-ray structure of the dysprosium analogues of **[(*S*)/(*R*)-1]$_n$**,[60] **[(*S,S,S*)/(*R,R,R*)-2]$_n$**, **[(*S*)/(*R*)-3]$_n$** and **[(*S,S,S*)/(*R,R,R*)-4]$_n$**.[55] The isomorphism of the Ytterbium derivatives and their purity phase were checked by single-crystal X-ray diffraction

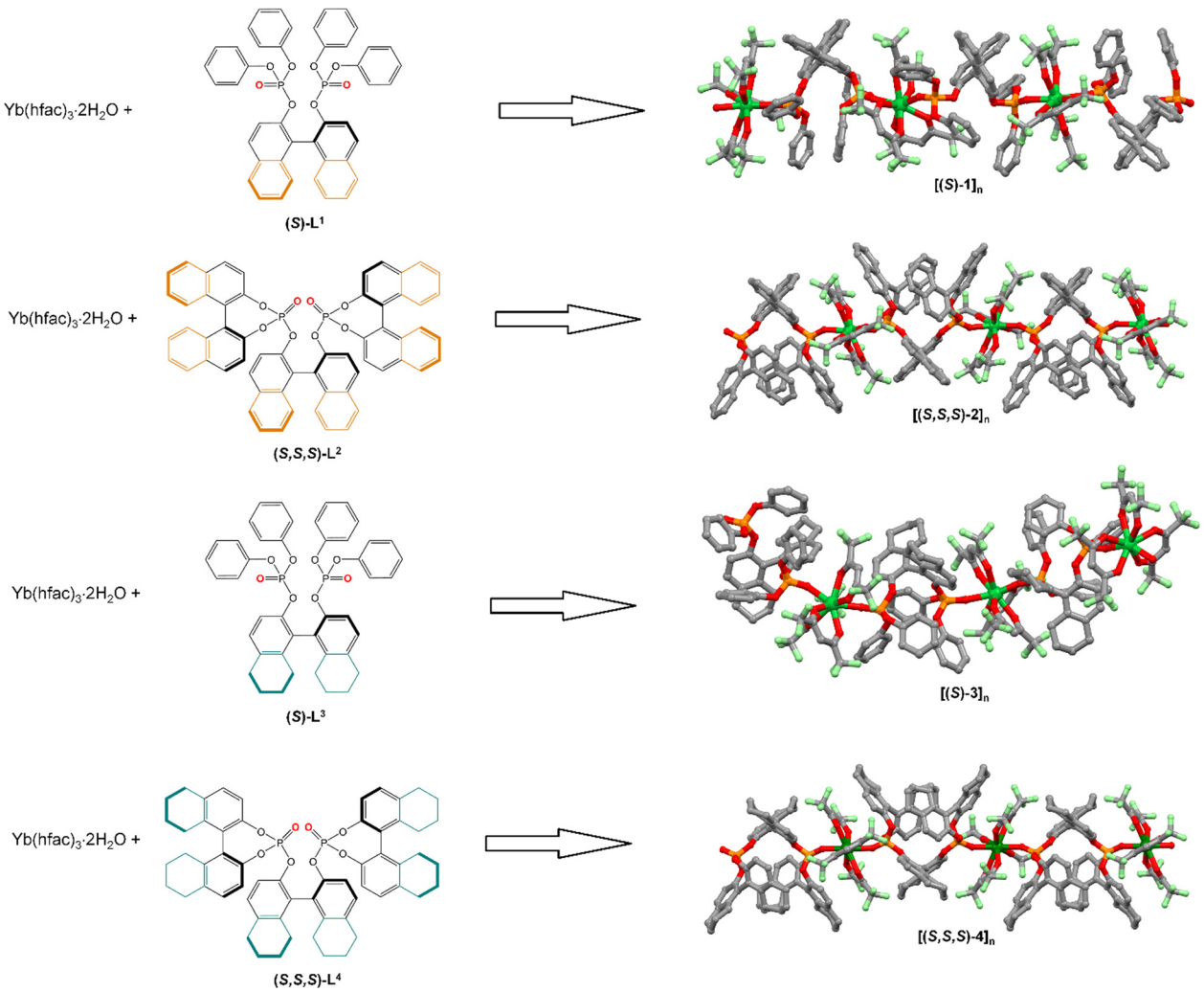

Scheme 1 Coordination reactions of the formation of **[(*S*)-1]$_n$**, **[(*S,S,S*)-2]$_n$**, **[(*S*)-3]$_n$** and **[(*S,S,S*)-4]$_n$** polymers with molecular structures of the (S)-enantiomer of the four ligands emphasizing the difference between the ligands. The **[(*S,S,S*)-4]$_n$** drawing was made from the X-ray structure of the dysprosium analogue.

(for the *S* enantiomers, (Fig. S1–S3 and Table S1, ESI†) and by powder X-ray diffraction for both enantiomers (Fig. S4, ESI†). For **[(*S,S,S*)-4]$_n$**, fast loss of crystallographic solvent molecules led to a loss of crystallinity of the powder, and a determination of the cell parameters was performed from a single crystal study (Table S2, ESI†).

The equimolar reaction of the Yb(hfac)$_3$(H$_2$O)$_2$ precursor and binaphtyl ligands led to the formation of one-dimensional polymeric structures (Scheme 1). The Yb(hfac)$_3$ units are bridged by the binaphtyl-based ligands *via* the P═O groups, and the Yb(III) ions are surrounded by eight oxygen atoms in a square antiprism coordination polyhedron (D$_{4d}$ symmetry). The cohesion of the crystal packing is assumed by both π–CH interactions and F···H contacts without π–π stacking.

Magnetic properties

Static magnetic investigations. The temperature dependences of $\chi_M T$ (where χ_M is the molar magnetic susceptibility and T is the temperature) for complexes **[(*S*)-1]$_n$**, **[(*S,S,S*)-2]$_n$**, **[(*S*)-3]$_n$** and **[(*S,S,S*)-4]$_n$** are shown in Fig. 1. The room temperature values are 2.46 cm^3 K mol^{-1}, 2.44 cm^3 K mol^{-1}, 2.46 cm^3 K mol^{-1} and 2.44 cm^3 K mol^{-1} for **[(*S*)-1]$_n$**, **[(*S,S,S*)-2]$_n$**, **[(*S*)-3]$_n$** and **[(*S,S,S*)-4]$_n$**, respectively. These values are close to the expected value of 2.57 cm^3 K mol^{-1} for one magnetically isolated Yb(III) ions with ground state multiplet $^2F_{7/2}$ and g_J = 8/7.[61] On cooling to 2 K, the $\chi_M T$ products decrease monotonically until the values of 1.60 cm^3 K mol^{-1}, 1.49 cm^3 K mol^{-1}, 1.64 cm^3 K mol^{-1} and 1.61 cm^3 K mol^{-1} for **[(*S*)-1]$_n$**, **[(*S,S,S*)-2]$_n$**, **[(*S*)-3]$_n$** and **[(*S,S,S*)-4]$_n$**, respectively. The field dependence of magnetization measured at 2K (inset of Fig. 1) agrees with the magnetic behaviour for the isolated Yb(III) centres. All the magnetization values at 50 kOe are close to 1.9 Nβ, which is far from the saturation values of 4 Nβ expected for one magnetically isolated Yb(III) ion, which is a sign of significant magnetic anisotropy.[61]

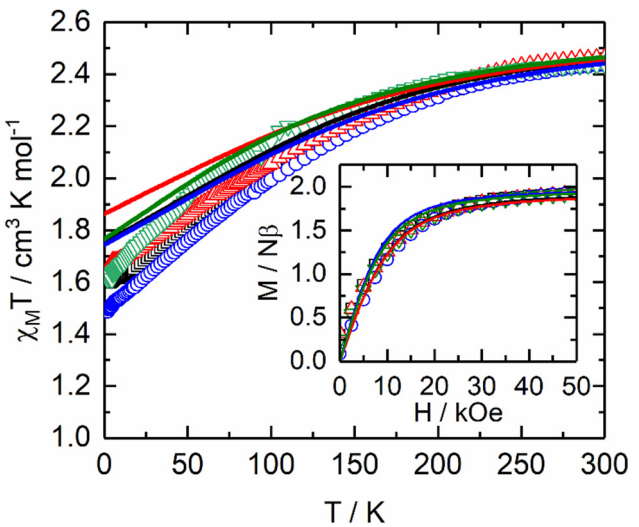

Fig. 1 Thermal dependence of $\chi_M T$ for (a) **[(*S*)-1]$_n$** (black squares), (b) **[(*S,S,S*)-2]$_n$** (blue circles), (c) **[(*S*)-3]$_n$** (red up-triangles) and (d) **[(*S,S,S*)-4]$_n$** (green down-triangles). Inset: Field variation of the magnetization measured at 2 K for **[(*S*)-1]$_n$** (black squares), (b) **[(*S,S,S*)-2]$_n$** (blue circles), (c) **[(*S*)-3]$_n$** (red up-triangles) and (d) **[(*S,S,S*)-4]$_n$** (green down-triangles). Full lines correspond to the *ab initio* computational results (see text for details).

To rationalize the magnetic properties of the polymers, SA-CASSCF/RASSI-SO calculations were performed on similar model systems previously used for the dysprosium analogues (see Computational details).[54,55] The experimental thermal dependence of $\chi_M T$ and field dependence of the magnetization were computed with the calculated energy splitting of the $^2F_{7/2}$ multiplet (Table S3, ESI†) and the composition of the ground doublet states (Fig. 1).

The temperature dependence of the magnetic susceptibility and the magnetic field dependence of the magnetization obtained from the *ab initio*-calculated energy levels agree fairly with the experimental ones for all complexes, confirming the correct crystal field splitting and the description of the ground state of these systems. The ground states are mainly composed of $|\pm 7/2>$ doublet, leading a to g$_z$ factor that ranges from 7.46 to 7.72 with significant non-zero transversal component values (Table 1).

Dynamic magnetic investigations. Dynamic magnetic measurements were performed to investigate slow magnetic relaxation behaviour. The field dependencies of the magnetic susceptibilities are shown in Fig. S5 (ESI†). In the absence of a static applied field, no out-of-phase χ_M'' component was observed for any compound. This is attributed to relaxation *via* fast Quantum Tunnelling of the Magnetization (QTM) due to the non-zero g_x and g_y components. QTM can be suppressed by applying an external magnetic field. Moreover, χ_M'' maxima were detected for all complexes under modest static fields. The magnetization relaxation times (τ) were extracted using an extended Debye model accounting for a single relaxation contribution (eqn. (S1), ESI†) for **[(*S*)-1]$_n$**, **[(*S*)-3]$_n$** and **[(*S,S,S*)-4]$_n$** (Table S4–S6, ESI†). The complex **[(*S*)-1]$_n$** with three crystallographic centres demonstrates only one contribution of magnetization relaxation, as already observed for its dysprosium analogue.[60] The broadness of the χ_M'' signal suggests the presence of multiple contributions for the relaxation of the magnetization of **[(*S,S,S*)-2]$_n$**. Thus, an extended Debye model considering two τ (eqn (S2), ESI†) was used (Table S7, ESI†) for **[(*S,S,S*)-2]$_n$**. This might be due to an intramolecular mechanism observed for [Dy(hfac)$_3$((*S*)-L^1)],[54] or to the loss of crystallization solvent molecules. The latter could induce a partial collapse of the crystal structure as a result of partial variation in atomic positions. The log(τ) *vs.* H plots are depicted in Fig. 2. The three compounds **[(*S*)-1]$_n$**, **[(*S*)-3]$_n$** and **[(*S,S,S*)-4]$_n$** and the high frequency (HF)

Table 1 Energy splitting of the $^2F_{7/2}$ multiplet state with composition and *g* factor values for each Kramers Doublet (KD)

Compounds	g_x	g_y	g_z	GS	Δ (cm^{-1})
[a]**[(*S*)-1]$_n$**	0.17	0.35	7.50	90%$\|\pm 7/2>$	261
[(*S,S,S*)-2]$_n$	0.09	0.11	7.72	95%$\|\pm 7/2>$	263
[(*S*)-3]$_n$	0.11	0.13	7.47	89%$\|\pm 7/2>$	280
[(*S,S,S*)-4]$_n$	0.49	0.73	7.46	91%$\|\pm 7/2>$	181

[a] The given values are the average values of the three crystallographically independent Yb(III) centres.

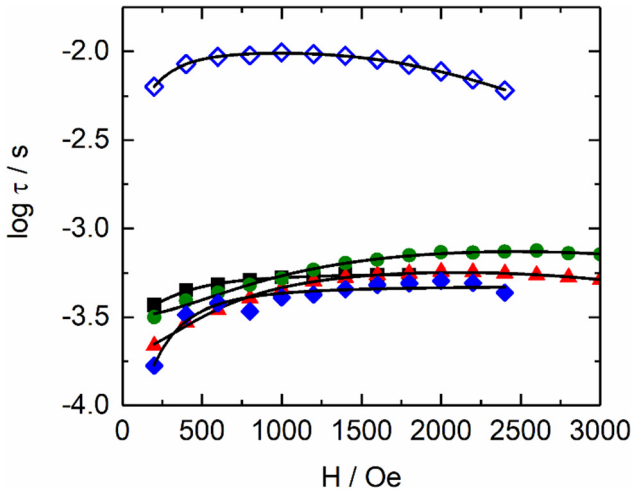

Fig. 2 Field dependence of the relaxation times for **[(*S*)-1]$_n$** (full black squares), **[(*S,S,S*)-2]$_n$** (full blue lozenges for LF contribution and empty blue lozenges for HF contribution)), **[(*S*)-3]$_n$** (full red up-triangles) and **[(*S,S,S*)-4]$_n$** (full green circles). Black lines are the best-fitted curves.

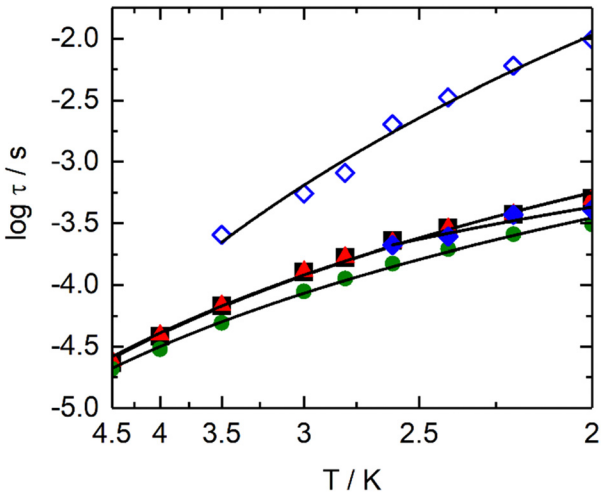

Fig. 3 Temperature variations in the relaxation times in the range of 2–4.5 K under 1000 Oe for **[(*S*)-1]$_n$** (full black squares), **[(*S,S,S*)-2]$_n$** (full blue lozenges for LF contribution and empty blue lozenges for HF contribution)), **[(*S*)-3]$_n$** (full red up-triangles) and **[(*S,S,S*)-4]$_n$** (full green circles). The black lines depict the best fits with the parameters given in the text.

contribution of **[(*S,S,S*)-2]$_n$** display similar τ field dependencies. Conversely, the low-frequency (LF) contribution for **[(*S,S,S*)-2]$_n$** exhibits a significantly slower magnetization relaxation rate. The log(τ) *vs.* H data can be fitted by eqn (1), and the fit parameters are shown in Table S8 (ESI†).

$$\tau^{-1}(T,H) = AH^4T + \frac{B_1}{1+B_2H^2} + \underbrace{\tau_0^{-1}e^{\left(\frac{U_{\text{eff}}}{k_BT}\right)}}_{k(T)} + CT^n \quad (1)$$

From left to right, the terms are the expressions of Direct, QTM and thermally activated (Orbach and Raman) contributions. As expected, the values of parameters for **[(*S*)-1]$_n$**, **[(*S*)-3]$_n$** and **[(*S,S,S*)-4]$_n$** are close to each other. Surprisingly, **[(*S,S,S*)-2]$_n$** presents a different behaviour because it has two contributions: HF and LF. Although the B_1 and $k(T)$ values for the HF parameter are close to those of the other three compounds, the values for the LF contribution are significantly different from the HF ones for **[(*S,S,S*)-2]$_n$** and the other compounds. Such differences highlight the singular magnetic behaviour for the LF contribution of **[(*S,S,S*)-2]$_n$**. In any case, the field dependence of the relaxation times, as depicted in the data in Table S8 (ESI†), suggests that at 1000 Oe, the tunnelling phenomena should be largely diminished for all compounds, but direct processes should not be strongly activated yet (Fig. S6, ESI†).

Thus, a field of 1000 Oe was selected to study the temperature dependence of the magnetic susceptibilities. For all compounds, the χ_M'' maxima clearly shift to higher frequencies as the temperature increases (Fig. S7, ESI†). The temperature variation in the magnetic susceptibility can be analysed in the framework of an extended Debye model accounting for a single τ (eqn (S1), ESI†) in the case of **[(*S*)-1]$_n$**, **[(*S*)-3]$_n$** and **[(*S,S,S*)-4]$_n$** (Tables S9–S11, ESI†). Normalized Argand plot attested that 95% of the samples are involved in slow magnetic relaxation (Fig. S8, ESI†). For **[(*S,S,S*)-2]$_n$**, an extended Debye model is used, considering two τ until 2.6 K and a single τ for higher temperatures (Table S12, ESI†). For **[(*S,S,S*)-2]$_n$**, satisfying fittings can be reached with eqn (1) by considering only Raman (CT^n) relaxation processes (Fig. 3). The fit parameters are shown in Table 2. The Raman process at a given temperature is similar for **[(*S*)-1]$_n$**, **[(*S,S,S*)-2]$_n$** (HF), **[(*S*)-3]$_n$** and **[(*S,S,S*)-4]$_n$**. In particular, the exponents display lower values than the expected theoretical one (n = 9).[62] Such deviations might suggest the participation of optical phonons (molecular vibration modes) in the relaxation processes.[63] Conversely, the parameters for the **[(*S,S,S*)-2]$_n$** (LF) contribution show significantly different values. The C parameter is three orders of magnitude lower than that of the other compounds. The n exponent is equal to 6.92(4), a value closer to the theoretical one, indicating a major involvement in acoustic phonons (lattice vibrations) in the relaxation mechanism. No general conclusions can be extracted, but the data seem to indicate that for similar systems, optical phonons could allow faster Raman magnetization relaxation than acoustic phonons.

Photo-physical Properties

UV visible absorption and CD investigations. The UV-visible absorption and ECD spectra for the complexes **[(*S/R*)-1]**, **[(*S,S,S/R,R,R*)-2]**, **[(*S/R*)-3]** and **[(*S,S,S/R,R,R*)-4]** in CH_2Cl_2 solution are presented in Fig. S9 (ESI†). The fragmentation of the polymeric structures upon solubilisation and the reorganisation of both

Table 2 Fit parameters for the Raman relaxation processes extracted from the τ temperature dependences

Compound	C/s^{-1} K^{-n}	n
[(*S*)-1]$_n$	124(1)	3.83(10)
[(*S,S,S*)-2]$_n$ (HF)	357(1)	2.71(48)
[(*S*)-3]$_n$	130(1)	3.78(9)
[(*S,S,S*)-4]$_n$	257(23)	3.47(8)
[(*S,S,S*)-2]$_n$ (LF)	0.77(28)	6.92(4)

hfac$^-$ anions and binaphtyl-based ligands was previously demonstrated by NMR studies and DFT calculations.[54] Thus, n = 1 for the complexes in the solution. The two UV-visible absorptions and ECD spectra are very similar to those observed for their Eu(III) analogues, and they are briefly described as reminders. The experimental absorption curves of the complexes are composed of broad bands localized at 30–37 000 cm^{-1} and 43–45 000 cm^{-1} (or higher energy for partially hydrogenated binaphtyl ligands), which are mainly attributed to the π–π* transitions of the binaphthyl-like moieties with a contribution of the π–π* transitions of the hfac$^-$ anions.[64]

The enantiomeric nature of the complexes in the CH_2Cl_2 solution at room temperature was confirmed by the ECD spectra. The ECD signals of the complexes with the fully aromatic ligands **[(*S*/*R*)-1]** and **[(*S,S,S*/*R,R,R*)-2]** appear more intense than those of the complexes involving partially hydrogenated binaphtyl-based ligands. The larger structural changes previously suggested after coordination to the Yb(hfac)$_3$ units for (*S*)/(*R*)-L^1 and (*S*)/(*R*)-L^3 than for (*S,S,S*)/(*R,R,R*)-L^2 and (*S,S,S*)/(*R,R,R*)-L^4 induce exaltations of the ECD signals centred at 30 000 cm^{-1} (333 nm) and 34 000 cm^{-1} (294 nm) for **[(*S*/*R*)-1]** and **[(*S*/*R*)-3]** similarly to what was observed for the Dy(III) and Eu(III) analogues.[54,64] The largest absolute values of the dissymmetry factor $|g_{abs}|$ display magnitude order of 10^{-3} (eqn (S3) and Table S13, ESI†).

In line with the exaltation of the low-energy ECD contributions after metal coordination, the complexes **[(*S*/*R*)-1]** (3.50×10^{-3} at 333 nm) and **[(*S*/*R*)-3]** (2.92×10^{-3} at 333 nm) display stronger $|g_{abs}|$ values than the corresponding free ligands at the same wavelength. Such an increase at 294–333 nm was not observed for the complexes **[(*S,S,S*/*R,R,R*)-2]** and **[(*S,S,S*/*R,R,R*)-4]**, and the maximum g_{abs} values are determined at a higher wavelength (3.61×10^{-3} for **[(*S,S,S*/*R,R,R*)-2]** at 260 nm) and (1.10×10^{-3} for **[(*S,S,S*/*R,R,R*)-4]** at 244 nm) (Table S13, ESI†).

Luminescence and CPL investigations. For all complexes, near-infrared (NIR) light emission can be detected upon excitation at 280 nm (35 714 cm^{-1}) in CH_2Cl_2 solution at room temperature. Such emission is characteristic of the $^2F_{5/2} \rightarrow {}^2F_{7/2}$ transition for a Yb(III) ion.[65] Thus, the four binaphtyl-based ligands can act as antennae chromophores for sensitization of the Yb(III) luminescence *via* the antenna effect mechanism.[66] The room temperature emission spectra in the CH_2Cl_2 solution are poorly resolved and

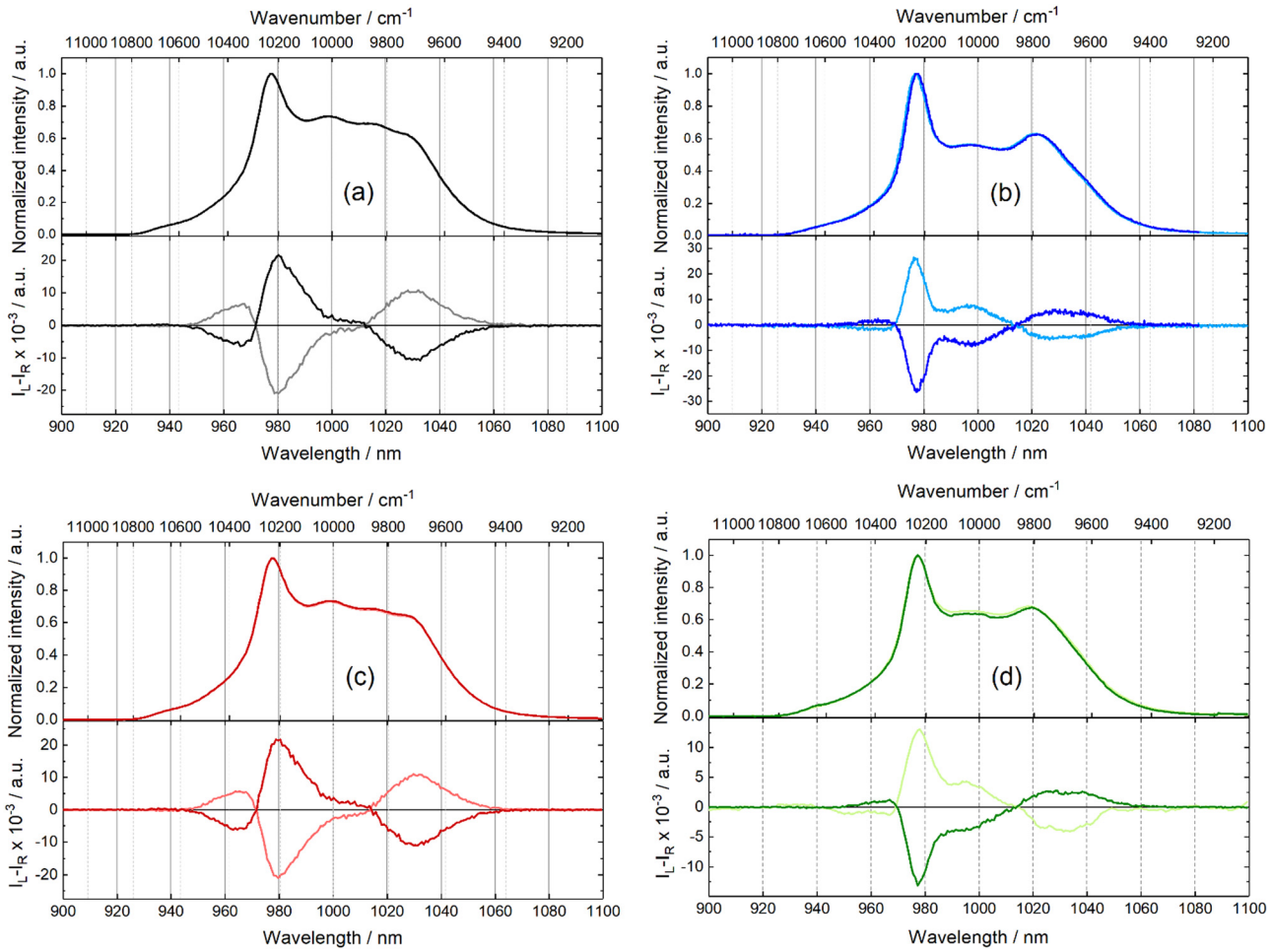

Fig. 4 Total emission (top) and CPL spectra (bottom) measured in CH_2Cl_2 solution under 280 nm (35 714 cm^{-1}) irradiation at room temperature for (a) **[(*S*)-1]** (gray line) and **[(*R*)-1]** (black line) ($C = 1 \times 10^{-5}$ mol L^{-1}), (b) **[(*S,S,S*)-2]** (light blue line) and **[(*R,R,R*)-2]** (dark blue line) ($C = 1 \times 10^{-5}$ mol L^{-1}), (c) **[(*S*)-3]** (light red line) and **[(*R*)-3]** (dark red line) ($C = 1 \times 10^{-4}$ mol L^{-1}) and (d) **[(*S,S,S*)-4]** (light green line) and **[(*R,R,R*)-4]** (dark green line) ($C = 5 \times 10^{-5}$ mol L^{-1}).

could be a consequence of additional contributions (hot bands) and vibrational motions.[58,67]

The emission decay curves can be fitted by mono-exponential functions (Fig. S10, ESI†), confirming the presence of a single spectroscopic Yb(III) site, thus supporting the existence of single monomeric species in the solution. The order of magnitude of the observed lifetimes (τ_{obs}) is the same for all the samples with τ_{obs} = 23.8 μs, 23.2 μs, 22.3 μs and 12.2 μs for **[(*S*/*R*)-1]**, **[(*S,S,S*/*R,R,R*)-2]**, **[(*S*/*R*)-3]** and **[(*S,S,S*/*R,R,R*)-4]**, respectively.

Symmetrical CPL signals are recorded for each enantiomeric pair (Fig. 4). Thus, the following discussion is given for (*S*) enantiomers. A clear correspondence between the CPL and luminescence transitions can be observed (Fig. 4) as well as similarities between the CPL spectra of the different compounds. All the CPL spectra are composed of four contributions localized around 965 nm (10 363 cm^{-1}), 980 nm (10 204 cm^{-1}), 995 nm (10 050 cm^{-1}) and 1030 nm (9709 cm^{-1}). Transitions from the ytterbium ion seem not to be environment dependent for the transition location in wavelength, while the CPL has many changes in relative intensities and signs, as described hereinafter. The shape of the CPL spectra, including the sign and intensity of the four contributions, is similar for the two **[(*S*)-1]** and **[(*S*)-3]** complexes as well as for the two **[(*S,S,S*)-2]** and **[(*S,S,S*)-4]** complexes. Hence, the general feature of the CPL spectra might be associated with the number of stereogenic elements, one for **[(*S*)-1]** and **[(*S*)-3]** and three for **[(*S,S,S*)-2]** and **[(*S,S,S*)-4]**, leading to different steric hindrances and variations in the coordination spheres around the Yb(III) centres. Interestingly, such observations were already made for Eu(III) analogues, demonstrating that the nature of the metal centres has no effect. To provide a more detailed description of the CPL spectra, one could observe that the four CPL contributions have positive/negative/negative/positive (+/−/−/+) sign for both **[(*S*)-1]** and **[(*S*)-3]** complexes, while the two other CPL spectra for **[(*S,S,S*)-2]** and **[(*S,S,S*)-4]** complexes have negative/positive/positive/negative (−/+/+/−) signs. Moreover, the highest-energy CPL contribution (corresponding to a hot band in the emission spectrum) is more intense for **[(*S*)-1]** and **[(*S*)-3]** than for **[(*S,S,S*)-2]** and **[(*S,S,S*)-4]**,

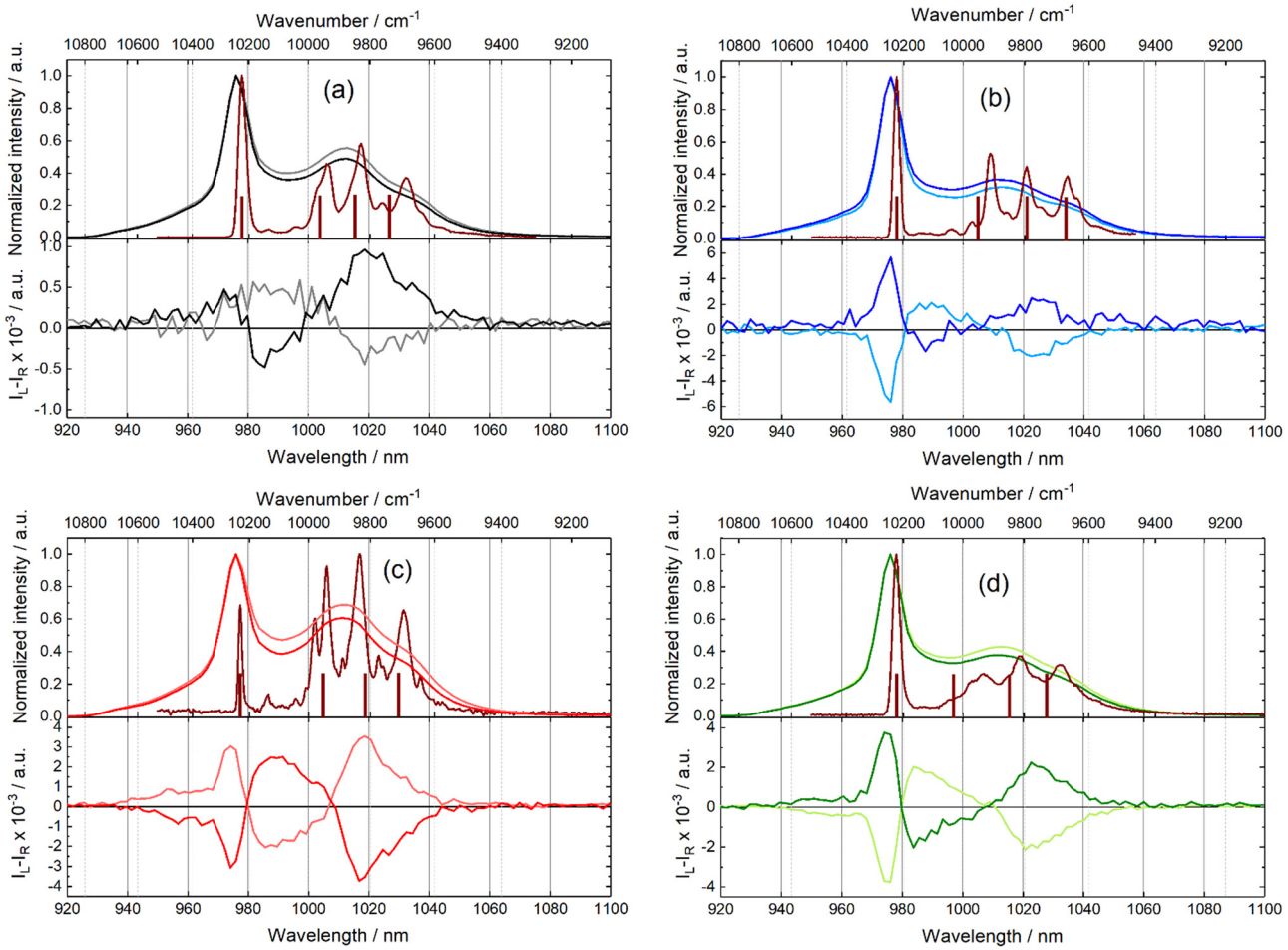

Fig. 5 (a) (top) Total emission and (bottom) CPL spectra measured in solid-state under 280 nm (35 714 cm^{-1}) irradiation at room temperature for **[(*S*)-1]**$_n$ (gray line) and **[(*R*)-1]**$_n$ (black line) (C = 1 × 10^{-5} mol L^{-1}), (b) **[(*S,S,S*)-2]**$_n$ (light blue line) and **[(*R,R,R*)-2]**$_n$ (dark blue line) (C = 1 × 10^{-5} mol L^{-1}), (c) **[(*S*)-3]**$_n$ (light red line) and **[(*R*)-3]**$_n$ (dark red line) (C = 1 × 10^{-4} mol L^{-1}) and (d) **[(*S,S,S*)-4]**$_n$ (light green line) and **[(*R,R,R*)-4]**$_n$ (dark green line) (C = 5 × 10^{-5} mol L^{-1}). (top) Total emission in solid-state under 350 nm (28 571 cm^{-1}) irradiation at 10 K (brown line) with vertical sticks representing the calculated energy splitting of the $^2F_{7/2}$ level for (a) **[(*S*)-1]**$_n$, (b) **[(*S,S,S*)-2]**$_n$, (c) **[(*S*)-3]**$_n$ and (d) **[(*S,S,S*)-4]**$_n$.

while the opposite trend is observed for the CPL contributions centred at 995 nm (10 050 cm^{-1}).

The g_{lum} values are presented in Table S13 (ESI†). The average maximum $|g_{lum}|$ values between the two enantiomers for **[(*S*/*R*)-1]** ($|^{max}g_{lum}| = 4.57 \times 10^{-2}$ at 980 nm), **[(*S*,*S*,*S*/*R*,*R*,*R*)-2]** ($|^{max}g_{lum}| = 5.23 \times 10^{-2}$ at 977 nm), **[(*S*/*R*)-3]** ($|^{max}g_{lum}| = 4.63 \times 10^{-2}$ at 982 nm) and **[(*S*,*S*,*S*/*R*,*R*,*R*)-4]** ($|^{max}g_{lum}| = 2.64 \times 10^{-2}$ at 978 nm) display comparable values, which are in range of classical g_{lum} value for Yb(III) coordination systems.[68–78] The nature of the ligand does not seem to affect the $|g_{lum}|$of the zero phonon line at 980 nm, while other transitions, for instance, the hot band localized at 960 nm, are more affected by the change in the ligand (Table S14, ESI†).

Considering that this series of Yb(III)-based complexes allowed us to observe slow magnetization relaxation in a solid state, optical studies are also presented for the complexes in a solid state. Moreover, the solid state allows emission measurements at a low temperature (10 K), which may help to define the crystal field splitting of the lanthanide ground state. Characteristic NIR Yb(III)-centred emission can be observed for all species upon excitation between 280 nm (35 714 cm^{-1}) at room temperature and 350 nm (28 571 cm^{-1}) at 10 K (Fig. 5). Therefore, the selected ligand systems act as antennas for the Yb(III) ion in the solid state. As observed in the solution, the NIR total emission spectra are scarcely resolved at room temperature (Fig. 5). Three contributions can be recognized in each spectrum centred at about 975 nm (10 256 cm^{-1}), 1012 nm (9881 cm^{-1}) and 1033 nm (9681 cm^{-1}). Low-temperature measurements at 10 K were performed for the four coordination polymers (*S* enantiomers). The resolution of the spectra improved considerably. Each spectrum at 10 K displays the four main signals expected at a $^2F_{5/2} \rightarrow {}^2F_{7/2}$ transition (Table S14, ESI†). The energy differences between each M_J doublets experimentally observed are equal to 285 cm^{-1}, 397 cm^{-1} and 540 cm^{-1} for **[(*S*)-1]*n***; 314 cm^{-1}, 431 cm^{-1} and 558 cm^{-1} for **[(*S*,*S*,*S*)-2]*n***; 295 cm^{-1}, 402 cm^{-1} and 539 cm^{-1} for **[(*S*)-3]*n*** and 290 cm^{-1}, 411 cm^{-1} and 535 cm^{-1} for **[(*S*,*S*,*S*)-4]*n***. Such total splitting values indicate low symmetrical coordination environments for the metal.[79,80] The minor differences observed between the spectra (*e.g.* splitting, shape, and relative peak intensities) might be attributed to the structural variations provoked by the enantiopure ligands. It is well known, since the pioneering work of Sessoli and coll,[81] that magneto-structural correlation can be done between magnetic properties and experimental luminescence for a wide selection of lanthanide ions.[21–23] Thus, the $^2F_{5/2} \rightarrow {}^2F_{7/2}$ energy splitting is compared to computed energy splitting. The calculation at the CASSCF level gave the energy splitting for the $^2F_{7/2}$ ground state depicted in the brown sticks in Fig. 5, which is in good agreement with the energy position of the emissive lines. The computed energy barrier values range from 181 cm^{-1} to 280 cm^{-1}, which are greater than the extracted values from the ac magnetic measurements, thereby confirming the absence of the Orbach process in the magnetic relaxation.

The differential emission between left and right circularly polarized light was detected for all Yb(III)-based complexes in the solid state at room temperature (Fig. 5). Almost symmetrical CPL spectra were recorded for each enantiomeric pair. The signal intensity for complex **[(*S*)/(*R*)-1]*n*** is particularly low, and the CPL contribution in correspondence of the emission band at 978 nm (10 256 cm^{-1}) is not clearly detected. Two CPL contributions can be unambiguously observed at approximately 985 nm (10 152 cm^{-1}) and 1020 nm (9804 cm^{-1}). All the other complexes present three well-defined CPL contributions with a fourth weak CPL contribution at 960 nm for **[(*S*)-3]*n*** (Fig. 5c) and **[(*S*,*S*,*S*)-4]*n*** (Fig. 5d). Both CPL signals at lower (975 nm) and higher (1020 nm) wavelengths are positioned in correspondence with the four peaks in the total emission. Conversely, the central CPL signals around 960 and 985 nm do not correspond with any main signal in the total emission. This is particularly well highlighted when compared with the total emission studies at 10 K. Based on these considerations, it might be tempting to assign these two CPL signals to "hot band" emissions. The g_{lum} values are close to 10^{-2} for **[(*S*,*S*,*S*)/(*R*,*R*,*R*)-2]*n***, **[(*S*)/(*R*)-3]*n*** and **[(*S*,*S*,*S*)/(*R*,*R*,*R*)-4]*n*** but weaker for **[(*S*)/(*R*)-1]*n*** (Table S15). The conversion of the polymeric nature of the compounds in solid-state into monomeric ones in CH_2Cl_2 solution did not induce any obvious relation between CPL measurements in solution and solid-state and did not allow rationalization for the inversion of CPL contribution signs from solution to solid-state for some compounds.[82–84]

Conclusions

In conclusion, the four Yb(III) polymeric analogues of formulas $\{[Yb(hfac)_3((S)/(R)\text{-}L^x)]\}_n$ (x = 1 and 3) and $\{[Yb(hfac)_3((S,S,S)/(R,R,R)\text{-}L^x)]\}_n$ (x = 2 and 4) are synthetized and characterized by SCXRD and PXRD, respectively. All the compounds displayed field-induced SMM behaviour in the solid state with slow magnetic relaxation occurring through the Raman process. The binaphtyl-based ligands acted as organic chromophores for the sensitization of the NIR $^2F_{5/2} \rightarrow {}^2F_{7/2}$ Yb(III) emission in both the solution and solid states. The magnetic properties are rationalized by *ab initio* calculations, and the computed crystal field splitting is rationalized by the magneto-structural correlation between magnetic and emissive properties. Finally, NIR-CPL was detected in both the solution and solid states. A correlation between the shape of the NIR-CPL and the nature of the chiral ligand could be done, but such an investigation is more complicated for solid-state measurements at this stage. This series of compounds can be classified as field-induced SMMs emitting CPL, and they are growing the short list of molecular systems that display both SMM and CPL behaviors.[57–59,85]

Experimental section

Materials

The precursors $Yb(hfac)_3(H_2O)_2$ ($hfac^-$ = 1,1,1,5,5,5-hexafluoroacetylacetonate anion),[86] $((S)/(R))\text{-}L^x$ (x = 1 and 3) and $((S,S,S)/(R,R,R))\text{-}L^x$ (x = 2 and 4) ligands[87] were synthesized following previously reported methods. All other reagents were purchased from Merck Co., Inc. and used without further purification.

Synthesis

$\{[Yb(hfac)_3((S)/(R)\text{-}L^1)]_3\}_n$ ($[(S)/(R)\text{-}1]_n$). 24.9 mg (0.03 mmol) of $[Yb(hfac)_3(H_2O)_2]$ were added to a solution containing 22.5 mg (0.03 mmol) of (*S*)-L^1 or (*R*)-L^1 in 1.5 mL of CH_2Cl_2. After 15 minutes of stirring, 60 mL of *n*-hexane were layered. After several days, the solution slowly evaporated, leading to a colourless and microcrystalline solid. 28.3 mg, 61% yield for **$[(S)\text{-}1]_n$** and 39.9 mg, 86% yield for **$[(R)\text{-}1]_n$**. Anal. Calcd (%) for $C_{177}H_{105}Yb_3F_{54}O_{42}P_6$ ($[(S)\text{-}1]_n$): C 45.83, H 2.27; found: C 45.94, H 2.33. Anal. Calcd (%) for $C_{177}H_{105}Yb_3F_{54}O_{42}P_6$ ($[(R)\text{-}1]_n$): C 45.83, H 2.27; found: C 45.87, H 2.31. I. R. (KBr, range 3200–400 cm^{-1}): 1656 (w), 1591 (m), 1558 (m), 1527 (m), 1501 (s), 1489 (s), 1456 (w), 1255 (s), 1191 (s), 1143 (s), 1102 (m), 1079 (m), 1029 (s), 1015 (s), 1005 (m), 994 (m), 966 (m), 951 (m), 902 (w), 875 (w), 869 (w), 850 (w), 807 (m), 796 (m), 779 (m), 763 (m), 753 (m), 740 (w), 704 (w), 686 (m), 662 (m), 615 (w), 585 (m), 558 (w), 554 (w), 526(w), 517 (w), 502(w), 495 (w), 482 (w), 464 (w) and 457 (w) cm^{-1} for **$[(S)\text{-}1]$** and for **$[(R)\text{-}1]$** (c = 1.0, $CHCl_3$).

$\{[Yb(hfac)_3((S,S,S)/(R,R,R))\text{-}L^2)]\}_n$ ($[(S,S,S)/(R,R,R)\text{-}2]_n$). A solution of 49.8 mg (0.06 mmol) of $[Yb(hfac)_3(H_2O)_2]$ in 5 mL of CH_2Cl_2 was added to a solution of 56.8 mg (0.06 mmol) of (*S,S,S*)-L^2 or (*R,R,R*)-L^2 in 5 mL of CH_2Cl_2. After 15 minutes of stirring, 30 mL of *n*-hexane were layered. Slow diffusion led to colourless single crystals that were suitable for X-ray studies. 74.4 mg, 71% yield in crystals for **$[(S,S,S)\text{-}2]_n$** and 81.7 mg, 78% yield in crystals for **$[(R,R,R)\text{-}2]_n$**. Anal. calcd (%) for $C_{75}H_{39}YbF_{18}O_{14}P_2$ **$[(S,S,S)\text{-}2]_n$**: C 51.72, H 2.24; found: C 51.81, H 2.29. I. R. Anal. calcd (%) for $C_{75}H_{39}YbF_{18}O_{14}P_2$ **$[(R,R,R)\text{-}2]_n$**: C 51.72, H 2.24; found: C 51.88, H 2.23. Representative I.R (KBr, range 1800–400 cm^{-1}): 1654 (s), 1593 (w), 1558 (m), 1530 (m), 1507 (m), 1466 (m), 1257 (s), 1204 (s), 1147 (s), 1102 (m), 1072 (m), 1038 (m), 1014 (m), 973 (m), 898 (w), 813 (m), 798 (w), 750 (w), 662 (m), 587 (w) and 572 (w) cm^{-1} for **$[(S,S,S)\text{-}2]$** and for **$[(R,R,R)\text{-}2]$** (c = 1.0, $CHCl_3$).

$\{[Yb(hfac)_3((S)/(R)\text{-}L^3)]\}_n$ ($[(S)/(R)\text{-}1]_n$). 24.9 mg (0.03 mmol) of $[Yb(hfac)_3(H_2O)_2]$ were added to a solution containing 22.8 mg (0.03 mmol) of (*S*)-L^3 or (*R*)-L^3 in 1.5 mL of CH_2Cl_2. After 15 minutes of stirring, 60 mL of *n*-hexane were layered. After several days, the solution slowly evaporated, leading to a colourless and microcrystalline solid. 39.1 mg, 84% yield for **$[(S)\text{-}3]_n$** and 41.9 mg, 90% yield for **$[(R)\text{-}3]_n$**. Anal. Calcd (%) for $C_{59}H_{43}YbF_{18}O_{14}P_2$ ($[(S)\text{-}3]_n$): C 45.59, H 2.77; found: C 45.64, H 2.79. Anal. Calcd (%) for $C_{59}H_{43}YbF_{18}O_{14}P_2$ ($[(S)\text{-}3]_n$): C 45.59, H 2.77; found: C 45.55, H 2.86. I. R. (KBr, range 3200–400 cm^{-1}): 3079 (w), 2936 (w), 2863 (w), 1655 (s), 1591 (w), 1557 (m), 1527 (m), 1491 (s), 1256 (s), 1201 (s), 1147 (s), 1102 (m), 1074 (m), 1027 (m), 1018 (m), 992 (m), 971 (w), 962 (w), 808 (w), 798 (m), 778 (w), 754 (m), 741 (w), 687 (w), 661 (m), 586 (m), 527 (w), 507 (w) and 466 (w) cm^{-1} for **$[(S)\text{-}3]$** and for **$[(R)\text{-}3]$** (c = 1.0, $CHCl_3$).

$\{[Yb(hfac)_3((S,S,S)/(R,R,R))\text{-}L^4)]\}_n$ ($[(S,S,S)/(R,R,R)\text{-}4]_n$). A solution of 5 mL of toluene containing 58.3 mg (0.06 mmol) of (*S,S,S*)-L^4 or (*R,R,R*)-L^4 was added to a suspension of 49.8 mg (0.06 mmol) of $[Yb(hfac)_3(H_2O)_2]$ in 3 mL of toluene. The resulting solution was stirred for 15 minutes. The slow diffusion of *n*-pentane led to colourless crystals suitable for X-ray studies. 65.8 mg, 62% yield in crystals for **$[(S,S,S)\text{-}4]_n$** and 59.4 mg, 56% yield in crystals for **$[(R,R,R)\text{-}4]_n$**. Anal. calcd (%) for $C_{75}H_{63}YbF_{18}O_{14}P_2$ ($[(S,S,S)\text{-}4]_n$): C 51.02, H 3.57; found: C 51.15, H 3.66. Anal. calcd (%) for $C_{75}H_{63}YbF_{18}O_{14}P_2$ ($[(R,R,R)\text{-}4]_n$): C 51.02, H 3.57; found: C 51.11, H 3.51. Representative I. R. (KBr, range 3200–400): 3079 (w), 2936 (w), 2863 (w), 1655 (s), 1591 (w), 1557 (m), 1527 (m), 1491 (s), 1256 (s), 1201 (s), 1147 (s), 1102 (m), 1074 (m), 1027 (m), 1018 (m), 992 (m), 971 (w), 962 (w), 808 (w), 798 (m), 778 (w), 754 (m), 741 (w), 687 (w), 661 (m), 586 (m), 527 (w), 507 (w) and 466 (w). for **$[(S,S,S)\text{-}4]$** and for **$[(R,R,R)\text{-}4]$** (c = 1.0, $CHCl_3$).

Material characterization

All solid-state characterization studies (elementary analysis, IR, PXRD, magnetic susceptibility and photophysical measurements) were performed on dried samples and are considered without solvent of crystallization. The elemental analyses of the compounds were performed at the Centre Régional de Mesures Physiques de l'Ouest, Rennes.

X-ray structure analysis

Single crystals were mounted using a D8 VENTURE Bruker-AXS diffractometer for data collection for **$[(S)\text{-}1]_n$**, **$[(S,S,S)\text{-}2]_n$** and **$[(S)\text{-}3]_n$** (Table S1, ESI†) and cell determination for **$[(S,S,S)\text{-}4]_n$** (Table S2) (MoKα radiation source, λ = 0.71073 Å) from the Centre de Diffractométrie X (CDIFX), Université de Rennes 1, France. Structures were solved with direct methods using the SHELXT Program[88] and refined with a full matrix least-squares method on F2 using the SHELXL-14/7 program.[89] Crystallographic data for the structure reported in this paper were deposited with the Cambridge Crystallographic Data Centre (insert CCDC 2238387–2238389† for **$[(S)\text{-}3]_n$**, **$[(S,S,S)\text{-}2]_n$** and **$[(S)\text{-}1]_n$**). Powder X-ray diffraction (PXRD) patterns for all samples were recorded at room temperature in the 2θ range of 5–30° with a step size of 0.026° and a scan time per step of 600 s using a PANalytical X'Pert Pro diffractometer (Cu-L2, L3 radiation, λ = 1.5418 Å, 40 kV, 40 mA, PIXcel 1D detector). Data collector and HighScore Plus software were used, respectively, for recording and analysing the patterns.

Spectroscopic analysis

Optical rotations were recorded using a PerkinElmer Model 341 polarimeter. Absorption spectra were recorded on a JASCO V-650 spectrophotometer in diluted solution using spectrophotometric grade solvents. Electronic circular dichroism (ECD) was measured on a Jasco J-815 Circular Dichroism Spectrometer (IFR140 facility – Biosit-Université de Rennes 1). Luminescence spectra were measured using a Horiba-Jobin Yvon Fluorolog-3 spectrofluorimeter equipped with a three-slit double grating monochromator. The solid samples (crystalline powders) were placed in quartz tubes (0.5 mm diameter) and inserted in a quartz dewar filled with liquid nitrogen. The excitation was provided by unpolarized light from a 450 W xenon CW lamp and detected at an angle of 90°. An 830 nm long-pass filter was placed between the sample and the detectors to avoid the presence of stray light due to excitation. Spectra were corrected for the emission spectral response (detector and grating). Near infra-red emissions were recorded using either a

liquid nitrogen cooled, solid indium/gallium/arsenic detector (850–1600 nm) or a Symphony® II CCD detector. For low-temperature measurements, the quartz tube containing the sample was sealed and set into an Oxford Instrument helium-cooled cryostat (Optistat CF2) inserted directly into the sample chamber of the spectrofluorimeter. For luminescence lifetimes, the sample was excited using a pulsed Nd:YAG laser (SpectraPhysics) operating at 10 Hz. Light emitted at right angles to the excitation beam was focused onto the slits of a monochromator (PTI120), which was used to select the appropriate wavelength. The growth and decay of the luminescence at selected wavelengths were detected using a Ge photodiode (Edinburgh Instruments, EI-P) and recorded using a digital oscilloscope (Tektronix TDS320) before being transferred for analysis. Luminescence lifetimes were obtained by iterative reconvolution of the detector response (obtained using a scatterer) with exponential components for the growth and decay of the metal-centred luminescence.

A homemade CPL apparatus based on a standard photoelastic modulator (PEM from Hinds company) – polarizer arrangement was used. The solid-state sample is placed between two quartz windows and excited with a focused low-cost unpolarised UV LED (wavelength at 365 nm, power 2 mW, from Roithner), placed around 45 degrees of the collection angle. The luminescent light is collected with a lens and directs to the PEM and the following Glan polarizer (neutral axes at 45 degrees of that of the PEM). A second lens focuses the light on the entrance slit of a monochromator (Cornerstone CS260 from Newport). A photomultiplier tube (H10330B-75 from Hamamatsu) is used as a detector, and the electric signal is measured by applying a Keythley multimeter for the DC signal UDC and a Standford SR830 LockIn amplifier for the 1f modulated signal U1F. The fluorescence signal is given by the DC part of the signal, while the CPL is the modulated U1F signal, corrected by sqrt(2) (as we measure the effective voltage) and $J1(2.405) \sim 0.519$ (where $J1$ is the first kind Bessel function of the first order for a PEM phase retardation amplitude of 2.405 radians). All the spectra were obtained with a resolution of 3 nm in the whole range for a step of 0.25nm and an integration time of 2.1 s.

Magnetic analysis

The dc magnetic susceptibility measurements were performed on a solid polycrystalline sample with a Quantum Design MPMS-XL SQUID magnetometer between 2 and 300 K in an applied magnetic field of 0.02 T for temperatures of 2–20 K, 0.2 T for temperatures of 20–80 K and 1T for temperatures of 80-300 K. AC magnetic susceptibility measurements were performed using a Quantum Design MPMS-XL SQUID for frequencies between 1 and 1000 Hz and a Quantum Design PPMS magnetometers for frequencies between 50 and 10 000 Hz. These measurements were all corrected for diamagnetic contribution, as calculated with Pascal's constants.

Computational details

Density Functional Theory (DFT) geometry optimisations were carried out on the Y^{III} parent molecule as implemented in the Gaussian 09 (revision D.01) package[90] using the PBE0 hybrid functional.[91,92] The atomic positions were extracted from the X-ray crystal structures of **[(*S*)-1]$_n$**, **[(*S,S,S*)-2]$_n$** and **[(*S*)-3]$_n$** and the dysprosium analogue of **[(*S,S,S*)-4]$_n$**. Only the hydrogen and fluorine positions were optimized, whereas the other atomic positions remained frozen. The « Stuttgart/Dresden » basis sets and effective core potentials were used to describe the yttrium atom,[93] whereas other atoms were described with the SVP basis sets.[92] The wavefunction theory calculations (WFT) were carried out using the OpenMolcas software package.[94] In these calculations, the complete active space self-consistent field[95] (CASSCF) approach was used to treat the static correlation effects arising from the partially filled 4f shell of the Yb(III) ion. The second-order Douglas–Kroll–Hess[96,97] scalar relativistic (SR) Hamiltonian was used to treat the scalar relativistic effects combined with the all-electron atomic natural orbital relativistically contracted (ANO-RCC) basis sets from the OpenMolcas library.[98–100] The basis sets were contracted to the triple–ζ plus polarization (TZP) quality for the Yb, O and N atoms bonded to the lanthanide (Yb = 25s22p15d11f4g2h/8s7p4d3f2g; O = 14s9p5d3f2g/4s3p2d1f; N = 14s9p5d3f2g/4s3p2d1f), and to the double–ζ plus polarization (DZP) quality for the atoms of the bridging ligand (C = 14s9p5d3f2g/3s2p1d; F = 14s9p5d3f2g/3s2p1d; and S = 17s12p5d4f2g/4s3p1d), while the rest of the atoms were treated with basis set contracted to the double–ζ quality (C = 14s9p5d3f2g/3s2p1d; H = 8s4p3d1f/2s). The calculations employed the state-averaged formalism at the SR level by considering the 7 doublet spin states arising from the 13 electrons spanning the seven 4f orbitals (*i.e.* CAS(13,7)). The spin-orbit coupling (SOC) was then introduced within a state interaction based on calculated SR states using the restricted active space state interaction (RASSI) approach.[101] The EPR g-factors were calculated according to ref. 102 as implemented in the RASSI module of OpenMolcas, while the magnetic susceptibility and magnetization calculations were performed using the Single-Aniso and Poly-Aniso routines of OpenMolcas as detailed in ref. 103.

Author contributions

C. A. M., B. L. and G. A. performed the organic syntheses and performed the coordination chemistry and crystallisations; V. D. realised the single crystal X-ray diffraction experiments and refined the X-ray structures; C. A. M. and O. C. performed and analysed the magnetic measurements. V. M. and B. L. G. performed the computational investigation. O.M., Y.G. and F. R. investigated the absorption and emission properties. C. A. M., C. G., S. G., A. B.-L. and B. B. carried out the chiroptical measurements and their interpretations. C. L. discussed the idea and the results and commented on the manuscript. F. P. conceived and designed the experiments and drove the writing of the article. All authors have read and agreed on the published version of the manuscript.

Conflicts of interest

There are no conflicts to declare.

Acknowledgements

This work was supported by CNRS, Université de Rennes, the European Research Council through the ERC-CoG 725184 MULTIPROSMM (project no. 725184) and the Agence Nationale de la Recherche (SMMCPL ANR-19-CE29-0012-02). Part of this work has been performed using the Spectroscopies-DCTP core facility (UMS Biosit, Université de Rennes 1- Campus de Villejean - 35043 RENNES Cedex, FRANCE). B.L.G. and V.M. thank the French GENCI/IDRIS-CINES centres for high-performance computing resources.

Notes and references

1 M. Mannini, F. Pineider, P. Sainctavit, C. Danieli, E. Otero, C. Sciancalepore, A. M. Talarico, M.-A. Arrio, A. Cornia, D. Gatteschi and R. Sessoli, *Nat. Mater.*, 2009, **8**, 194.
2 S. Thiele, F. Balestro, R. Ballou, S. Klyatskaya, M. Ruben and W. Wernsdorfer, *Science*, 2014, **344**, 1135.
3 K. S. Pedersen, A.-M. Ariciu, S. McAdams, H. Weihe, J. Bendix, F. Tuna and S. Piligkos, *J. Am. Chem. Soc.*, 2016, **138**, 5801.
4 R. A. Layfield, M.-L. Tong, B. M. Day, Y.-C. Chen, F.-S. Guo and A. Mansikkamaki, *Science*, 2018, **362**, 1400.
5 K. Randall McClain, C. A. Gould, K. Chakarawet, S. J. Teat, T. J. Groshens, J. R. Long and B. G. Harvey, *Chem. Sci.*, 2018, **9**, 8492.
6 C. A. P. Goodwin, F. Ortu, D. Reta, N. F. Chilton and D. P. Mills, *Nature*, 2017, **548**, 439.
7 A. H. Vincent, Y. L. Whyatt, N. F. Chilton and J. R. Long, *J. Am. Chem. Soc.*, 2023, **145**, 1572.
8 J.-C. G. Bünzli, *Acc. Chem. Res.*, 2006, **39**, 53.
9 S. V. Eliseeva and J.-C. G. Bünzli, *Chem. Soc. Rev.*, 2010, **39**, 189.
10 S. V. Eliseeva and J.-C. G. Bünzli, in Lanthanide spectroscopy, Materials, and Bioapplications, *Springer Series on Fluorescence*, ed. Hännen, P., Härmä, H., Springer, Verlag, Berlin, 2010, vol. 7; in *Luminescence of Lanthanide Ions in Coordination Compounds and Nanomaterials*, ed. De Bettencourt-Diaz, A., Wiley, New York, 2014.
11 C. P. Montgomery, B. S. Murray, E. J. New, R. Pal and D. Parker, *Acc. Chem. Res.*, 2009, **42**, 925.
12 E. G. Moore, A. P. S. Samuel and K. N. Raymond, *Acc. Chem. Res.*, 2009, **42**, 542.
13 A. D'Aleo, A. Bourdolle, S. Bulstein, T. Fauquier, A. Grichine, A. Duperray, P. L. Baldeck, C. Andraud, S. Brasselet and O. Maury, *Angew. Chem., Int. Ed.*, 2012, **51**, 6622.
14 S. Banerjee, L. Huebner, M. D. Romanelli, G. A. Kumar, R. E. Riman, T. J. Emge and J. G. Brennan, *J. Am. Chem. Soc.*, 2005, **127**, 15900.
15 G. A. Kumar, R. E. Riman, L. A. Diaz Torres, S. Banerjee, M. D. Romanelli, T. J. Emge and J. G. Brennan, *Chem. Mater.*, 2007, **19**, 2937.
16 S. Banerjee, G. A. Kumar, R. E. Riman, T. J. Emge and J. G. Brennan, *J. Am. Chem. Soc.*, 2007, **129**, 5926.
17 M. Romanelli, G. A. Kumar, T. J. Emge, R. E. Riman and J. G. Brennan, *Angew. Chem., Int. Ed.*, 2008, **47**, 6049.
18 L. Song, X. Liu, Z. Zhen, C. Chen and D. Zhang, *J. Mater. Chem.*, 2007, **17**, 4586.
19 M. D. McGehee, T. Bergstedt, C. Zhang, A. P. Saab, M. B. O'Regan, G. C. Bazan, V. I. Srdanov and A. J. Heeger, *Adv. Mater.*, 1999, **11**, 1349.
20 A. de Bettencourt-Dias, *Dalton Trans.*, 2007, 2229.
21 F. Pointillart, B. Le Guennic, O. Cador, O. Maury and L. Ouahab, *Acc. Chem. Res.*, 2015, **48**, 2834.
22 J. H. Jia, Q.-W. Li, Y.-C. Chen, J.-L. Liu and M.-L. Tong, *Coord. Chem. Rev.*, 2019, **378**, 365–381.
23 R. Marin, G. Brunet and M. Murugesu, *Angew. Chem., Int. Ed.*, 2021, **60**, 1728.
24 X.-L. Li, C.-L. Chen, H.-P. Xiao, A.-L. Wang, C.-M. Liu, X. Zheng, L.-J. Gao, X.-G. Yanga and S.-M. Fang, *Dalton Trans.*, 2013, **42**, 15317.
25 J. Long, R. Vallat, R. A. S. Ferreira, L. D. Carlos, F. A. Almeida Paz, Y. Guari and J. Larionova, *Chem. Commun.*, 2012, **48**, 9974.
26 F. Pointillart, B. Le Guennic, T. Cauchy, S. Golhen, O. Cador, O. Maury and L. Ouahab, *Inorg. Chem.*, 2013, **52**, 5978.
27 M. Ren, S.-S. Bao, B.-W. Wang, R. A. S. Ferreira, L.-M. Zheng and L. D. Carlos, *Inorg. Chem. Front.*, 2015, **2**, 558.
28 G. Brunet, R. Marin, M. Monk, U. Resch-Genger, D. A. Galico, F. A. Sigoli, E. A. Suturina, E. Hemmer and M. Murugesu, *Chem. Sci.*, 2019, **10**, 6799.
29 D. Guettas, F. Gendron, G. Fernandez Garcia, F. Riobé, T. Roisnel, O. Maury, G. Pilet, O. Cador and B. Le Guennic, *Chem. – Eur. J.*, 2020, **26**, 4389.
30 G. L. J. A. Rikken and E. Raupach, *Nature*, 1997, **390**, 493.
31 B. Casanovas, S. Speed, M. S. El Fallah, R. Vicente, M. Font-Bardia, F. Zinna and L. Di Bari, *Dalton Trans.*, 2019, **48**, 2059.
32 D.-P. Li, T.-W. Wang, C.-H. Li, D.-S. Liu, Y.-Z. Li and X.-Z. You, *Chem. Commun.*, 2010, **46**, 2929.
33 X.-L. Li, C.-L. Chen, Y.-L. Gao, C.-M. Liu, X.-L. Feng, Y.-H. Gui and S.-M. Fang, *Chem. – Eur. J.*, 2012, **18**, 14632.
34 X.-L. Li, C.-L. Chen, H.-P. Xiao, A.-L. Wang, C.-M. Liu, X. Zheng, L.-J. Gao, X.-G. Yang and S.-M. Fang, *Dalton Trans.*, 2013, **42**, 15317.
35 J. Long, J. Rouquette, J.-M. Thibaud, R. A. R. Ferreira, L. D. Carlos, B. Donnadieu, V. Vieru, L. F. Chibotaru, L. Konczewicz, J. Haines, Y. Guari and J. Larionova, *Angew. Chem., Int. Ed.*, 2015, **54**, 2236.
36 X.-L. Li, M. Hu, Z. Yin, C. Zhu, C.-M. Liu, H.-P. Xiao and S. Fang, *Chem. Commun.*, 2017, **53**, 3998.
37 J. Long, M. S. Ivanov, V. A. Khomchenko, E. Mamontova, J.-M. Thibaud, J. Rouquette, M. Beaudhuin, D. Granier, R. A. S. Ferreira, L. D. Carlos, B. Donnadieu, M. S. C. Henriques, J. A. Paixao, Y. Guari and J. Larionova, *Science*, 2020, **367**, 671.
38 K. Wang, S. Zeng, H. Wang, J. Dou and J. Jiang, *Inorg. Chem. Front.*, 2014, **1**, 167.
39 M. Atzori, K. Dhbaibi, H. Douib, M. Grasser, V. Dorcet, I. Breslavetz, K. Paillot, O. Cador, G. L. J. A. Rikken, B. Le Guennic, J. Crassous, F. Pointillart and C. Train, *J. Am. Chem. Soc.*, 2021, **143**, 2671.

40 J. P. Riehl and F. S. Richardson, *Chem. Rev.*, 1986, **86**, 1.
41 R. Carr, N. H. Evans and D. Parker, *Chem. Soc. Rev.*, 2012, **41**, 7673.
42 H. Urey, K. V. Chellappan, E. Erden and P. Surman, *Proc. IEEE*, 2011, **99**, 540.
43 C. H. Bennett and D. P. DiVincenzo, *Nature*, 2000, **404**, 247.
44 L. Jennings, R. S. Waters, R. Pal and D. Parker, *ChemMedChem*, 2017, **12**, 271.
45 E. R. Neil, M. A. Fox, R. Pal and D. Parker, *Dalton Trans.*, 2016, **45**, 8355.
46 P. M. Burrezo, V. G. Jiménez, D. Blasi, I. Ratera, A. G. Campana and J. Veciana, *Angew. Chem., Int. Ed.*, 2019, **58**, 16282.
47 H. Isla, N. Saleh, J. K. Ou-Yang, K. Dhbaibi, M. Jean, M. Dziurka, L. Favereau, N. Vanthuyne, L. Toupet, B. Jamoussi, M. Srebro-Hooper and J. Crassous, *J. Org. Chem.*, 2019, **84**, 5383.
48 L. Guy, M. Mosser, D. Pitrat, J.-C. Mulatier, M. Kukulka, M. Srebro-Hooper, E. Jeanneau, A. Benslah-Ledoux, B. Baguenard and S. Guy, *J. Org. Chem.*, 2019, **84**, 10870.
49 Y. B. Tan, Y. Okayasu, S. Katao, Y. Nishikawa, F. Asanoma, M. Yamada, J. Yuasa and T. Kawai, *J. Am. Chem. Soc.*, 2020, **142**, 17653.
50 J. L. Lunkley, D. Shirotani, K. Yamanari, S. Kaizaki and G. Muller, *J. Am. Chem. Soc.*, 2008, **130**, 13814.
51 O. G. Willis, F. Zinna, G. Pescitelli, C. Micheletti and L. Di Bari, *Dalton Trans.*, 2022, **51**, 518.
52 N. F. M. Mukthar, N. D. Schley and G. Ung, *J. Am. Chem. Soc.*, 2022, **144**, 6148.
53 B.-A. N. Willis, D. Schnable, N. D. Schley and G. Ung, *J. Am. Chem. Soc.*, 2022, **144**, 22421.
54 C. A. Mattei, V. Montigaud, F. Gendron, S. Denis-Quanquin, V. Dorcet, N. Giraud, F. Riobé, G. Argouarch, O. Maury, B. Le Guennic, O. Cador, C. Lalli and F. Pointillart, *Inorg. Chem. Front.*, 2021, **8**, 947.
55 C. A. Mattei, V. Montigaud, V. Dorcet, F. Riobé, G. Argouarch, O. Maury, B. Le Guennic, O. Cador, C. Lalli and F. Pointillart, *Inorg. Chem. Front.*, 2021, **8**, 963.
56 C. Andrea Mattei, K. Dhbaibi, B. Lefeuvre, V. Dorcet, G. Argouarch, O. Cador, B. Le Guennic, O. Maury, C. Lalli, S. Guy, A. Bensalah-Ledoux, F. Riobé, B. Baguenard and F. Pointillart, *Chirality*, 2022, **34**, 34.
57 F. Gendron, S. Di Pietro, L. Abad Galán, F. Riobé, V. Placide, L. Guy, F. Zinna, L. Di Bari, A. Bensalah-Ledoux, Y. Guyot, G. Pilet, F. Pointillart, B. Baguenard, S. Guy, O. Cador, O. Maury and B. Le Guennic, *Inorg. Chem. Front.*, 2021, **8**, 914.
58 B. Lefeuvre, C. A. Mattei, J. Flores Gonzalez, F. Gendron, V. Dorcet, F. Riobé, C. Lalli, B. Le Guennic, O. Cador, O. Maury, S. Guy, A. Bensalah-Ledoux, B. Baguenard and F. Pointillart, *Chem. – Eur. J.*, 2021, **27**, 7362.
59 K. Dhbaibi, M. Grasser, H. Douib, V. Dorcet, O. Cador, N. Vanthuyne, F. Riobé, O. Maury, S. Guy, A. Bensalah-Ledoux, B. Baguenard, G. L. J. A. Rikken, C. Train, B. Le Guennic, M. Atzori, F. Pointillart and J. Crassous, *Angew. Chem., Int. Ed.*, DOI: **10.1002/anie.202215558**.
60 C. A. Mattei, B. Lefeuvre, V. Dorcet, G. Argouarch, O. Cador, C. Lalli and F. Pointillart, *Magnetochemistry*, 2021, **7**, 150.
61 C. Benelli and D. Gatteschi, *Introduction to Molecular Magnetism: From Transition Metals to Lanthanides*, Wiley-VCH Verlag GmbH & Co, KGaA, 2015.
62 J. Tang and P. Zhang, Lanthanide Single-Ion Molecular Magnets, *Lanthanide Single Molecule Magnets*, Springer, Verlag, Berlin, Heidelberg, 2015.
63 E. Rousset, M. Piccardo, M.-E. Boulon, R. W. Gable, A. Soncini, L. Sorace and C. Boskovic, *Chem. – Eur. J.*, 2018, **24**, 14768.
64 F. Pointillart, J. Jung, R. Berraud-Pache, B. Le Guennic, V. Dorcet, S. Golhen, O. Cador, O. Maury, Y. Guyot, S. Decurtins, S.-X. Liu and L. Ouahab, *Inorg. Chem.*, 2015, **54**, 5384.
65 L. Di Bari, G. Pintacuda and P. Salvadori, *J. Am. Chem. Soc.*, 2000, **122**, 5557.
66 *Molecular Magnetic Materials: Concepts and Applications*, ed. B. Sieklucka and D. Pinkowicz, Wiley-VCH Verlag GmbH & Co, KGaA, 2017.
67 K. S. Pedersen, J. Dreiser, H. Weihe, R. Sibille, H. V. Johannesen, M. A. Sorensen, B. E. Nielsen, M. Sigrist, H. Mutka, S. Rols, J. Bendix and S. Piligkos, *Inorg. Chem.*, 2015, **54**, 7600.
68 F. Zinna, L. Arrico and L. Di Bari, *Chem. Commun.*, 2019, **55**, 6607.
69 R. S. Dickins, J. A. K. Howard, C. L. Maupin, J. M. Moloney, D. Parker, J. P. Riehl, G. Siligardi and J. A. G. Williams, *Chem. – Eur. J.*, 1999, **5**, 1095.
70 J. W. Walton, R. Carr, N. H. Evans, A. M. Funk, A. M. Kenwright, D. Parker, D. S. Yufit, M. Botta, S. De Pinto and K. Wong, *Inorg. Chem.*, 2012, **51**, 8042.
71 C. L. Maupin, R. S. Dickins, L. G. Govenlock, C. E. Mathieu, D. Parker, J. A. G. Williams and J. P. Riehl, *J. Phys. Chem. A*, 2000, **104**, 6709.
72 R. Berardozzi and L. Di Bari, *ChemPhysChem*, 2015, **16**, 2868.
73 T. Wu, J. Kapitán, V. Andrushchenko and P. Bouř, *Anal. Chem.*, 2017, **89**, 5043.
74 T. Wu and P. Bour, *Chem. Commun.*, 2018, **54**, 1790.
75 T. Y. Bing, T. Kawai and J. Yuasa, *J. Am. Chem. Soc.*, 2018, **140**, 3683.
76 L. Dai, C. M. Jones, W. T. K. Chan, T. A. Pham, X. Ling, E. Gale, N. J. Rotile, W. C. Tai, C. J. Anderson, P. Caravan and G. Law, *Nat. Commun.*, 2018, **9**, 857.
77 J. Dai, J. Zhang, Y. Chen, M. E. Mackenzie, R. Pal and G.-L. Law, *Inorg. Chem.*, 2019, **58**, 12506.
78 C. L. Maupin, D. Parker, J. A. G. Williams and J. P. Riehl, *J. Am. Chem. Soc.*, 1998, **120**, 10563.
79 Y. Kishi, L. Cornet, F. Pointillart, F. Riobé, B. Lefeuvre, O. Cador, B. Le Guennic, O. Maury, H. Fujiwara and L. Ouahab, *Eur. J. Inorg. Chem.*, 2018, 458.
80 F. Guégan, J. Jung, B. Le Guennic, F. Riobé, O. Maury, B. Gillon, J.-F. Jacquot, Y. Guyot, C. Morel and D. Luneau, *Inorg. Chem. Front.*, 2019, **6**, 3152.

81 G. Cucinotta, M. Perfetti, J. Luzon, M. Etienne, P. E. Car, A. Caneschi, G. Calvez, K. Bernot and R. Sessoli, *Angew. Chem., Int. Ed.*, 2012, **51**, 1606.
82 Y. Nagata, T. Nishikawa and M. Suginome, *Chem. Commun.*, 2014, **50**, 9951.
83 Y. Sheng, J. Ma, S. Liu, Y. Wang, C. Zhu and Y. Cheng, *Chem. – Eur. J.*, 2016, **22**, 9519.
84 T. Kimoto, T. Amako, N. Tajima, R. Kuroda, M. Fujiki and Y. Imai, *Asian J. Org. Chem.*, 2013, **2**, 404.
85 B. El Rez, J. Liu, V. Béreau, C. Duhayon, Y. Horino, T. Suzuki, L. Coolen and J.-P. Sutter, *Inorg. Chem. Front.*, 2020, **7**, 4527.
86 M. F. Richardson, W. F. Wagner and D. E. Sands, *Inorg. Nucl. Chem.*, 1968, **30**, 1275.
87 A. Ngo Ndimba, T. Roisnel, G. Argouarch and C. Lalli, *Synthesis*, 2019, 865.
88 G. M. Sheldrick, *Acta Crystallogr., Sect. A: Found. Adv.*, 2015, **71**, 3.
89 G. M. Sheldrick, *Acta Crystallogr., Sect. C: Struct. Chem.*, 2015, **71**, 3.
90 M. J. Frisch, G. W. Trucks, H. B. Schlegel, G. E. Scuseria, M. A. Robb, J. R. Cheeseman, G. Scalmani, V. Barone, B. Mennucci, G. A. Petersson, *et al.*, *Gaussian 09 Revision, A.02*, Gaussian Inc., Wallingford, CT, USA, 2009.
91 J. P. Perdew, K. Burke and M. Ernzerhof, *Phys. Rev. Lett.*, 1996, **77**, 3865.
92 C. Adamo and V. Barone, *J. Chem. Phys.*, 1999, **110**, 6158.
93 F. Weigend and R. Ahlrichs, *Phys. Chem. Chem. Phys.*, 2005, **7**, 3297.
94 I. Fdez. Galván, M. Vacher, A. Alavi, C. Angeli, F. Aquilante, J. Autschbach, J. J. Bao, S. I. Bokarev, N. A. Bogdanov, R. K. Carlson, L. F. Chibotaru, J. Creutzberg, N. Dattani, M. G. Delcey, S. S. Dong, A. Dreuw, L. Freitag, L. M. Frutos, L. Gagliardi, F. Gendron, A. Giussani, L. González, G. Grell, M. Guo, C. E. Hoyer, M. Johansson, S. Keller, S. Knecht, G. Kovačević, E. Källman, G. Li Manni, M. Lundberg, Y. Ma, S. Mai, J. P. Malhado, P. Å. Malmqvist, P. Marquetand, S. A. Mewes, J. Norell, M. Olivucci, M. Oppel, Q. M. Phung, K. Pierloot, F. Plasser, M. Reiher, A. M. Sand, I. Schapiro, P. Sharma, C. J. Stein, L. K. Sørensen, D. G. Truhlar, M. Ugandi, L. Ungur, A. Valentini, S. Vancoillie, V. Veryazov, O. Weser, T. A. Wesołowski, P.-O. Widmark, S. Wouters, A. Zech, J. P. Zobel and R. Lindh, *J. Comput. Chem.*, 2019, **15**, 5925.
95 B. O. Roos, P. R. Taylor and P. E. M. Siegbahn, *Chem. Phys.*, 1980, **48**, 157.
96 M. Douglas and N. M. Kroll, *Ann. Phys.*, 1974, **82**, 89.
97 B. A. Hess, *Phys. Rev. A: At., Mol., Opt. Phys.*, 1985, **32**, 763.
98 P.-O. Widmark, P.-A. Malmqvist and B.-O. Roos, *Theor. Chim. Acta*, 1990, **77**, 291.
99 B. O. Roos, R. Lindh, P.-A. Malmqvist, V. Veryazov and P.-O. Widmark, *J. Phys. Chem. A*, 2004, **108**, 2851.
100 B. O. Roos, R. Lindh, P.-A. Malmqvist, V. Veryazov and P.-O. Widmark, *J. Phys. Chem. A*, 2005, **109**, 6575.
101 P.-A. Malmqvist, B. O. Roos and B. Schimmelpfennig, *Chem. Phys. Lett.*, 2002, **357**, 230.
102 H. Bolvin, *ChemPhysChem*, 2006, **7**, 1575.
103 L. F. Chibotaru and L. Ungur, *J. Chem. Phys.*, 2012, **137**, 064112.

